Theor Chem Acc (2011) 130:1231–1238
DOI 10.1007/s00214-011-0925-9

REGULAR ARTICLE

High-wavenumber FT-Raman spectroscopy for in vivo and ex vivo measurements of breast cancer

A. F. García-Flores · L. Raniero · R. A. Canevari · K. J. Jalkanen · R. A. Bitar · H. S. Martinho · A. A. Martin

Received: 13 September 2010 / Accepted: 14 March 2011 / Published online: 6 April 2011

Abstract The identification of normal and cancer breast tissue of rats was investigated using high-frequency (HF) FT-Raman spectroscopy with a near-infrared excitation source on in vivo and ex vivo measurements. Significant differences in the Raman intensities of prominent Raman bands of lipids and proteins structures (2,800–3,100 cm^{-1}) as well as in the broad band of water (3,100–3,550 cm^{-1}) were observed in mean normal and cancer tissue spectra. The multivariate statistical analysis methods of principal components analysis (PCA) and linear discriminant analysis (LDA) were performed on all high-frequency Raman spectra of normal and cancer tissues. LDA results with the leave-one-out cross-validation option yielded a discrimination accuracy of 77.2, 83.3, and 100% for in vivo transcutaneous, in vivo skin-removed, and ex vivo biopsy HF Raman spectra. Despite the lower discrimination value for the in vivo transcutaneous measurements, which could be explained by the breathing movement and skin influences, our results showed good accuracy in discriminating between normal and cancer breast tissue samples. To support this, the calculated integration areas from the receiver-operating characteristic (ROC) curve yielded 0.86, 0.94, and 1.0 for in vivo transcutaneous, in vivo skin-removed, and ex vivo biopsy measurements, respectively. The feasibility of using HF Raman spectroscopy as a clinical diagnostic tool for breast cancer detection and monitoring is due to no interfering contribution from the optical fiber in the HF Raman region, the shorter acquisition time due to a more intense signal in the HF Raman region, and the ability to distinguish between normal and cancerous tissues.

Keywords Raman spectroscopy · Breast cancer detection · Multivariate statistical analysis · Principal components analysis · Linear discriminant analysis · High frequency Raman

Abbreviations

BLR	Binary logistic regression
COBEA	Brazilian college of animal experimentation
CTT	Cancer tissue transcutaneous
DMBA	7,12-dimethylbenz(a)anthracene
EVCT	Ex vivo cancer tissue
EVNT	Ex vivo normal tissue
FT	Fourier transform
HF	High frequency
INCA	National institute for cancer
HM	Mammary hyperplasia
IR	Infrared
IVCT	In vivo cancer tissue
IVNT	In vivo normal tissue

Dedicated to Professor Akira Imamura on the occasion of his 77th birthday and published as part of the Imamura Festschrift Issue.

A. F. García-Flores · L. Raniero · R. A. Canevari · K. J. Jalkanen · A. A. Martin (✉)
Laboratory of Biomedical Vibrational Spectroscopy, Institute of Research and Development, IP&D, Universidade do Vale do Paraíba, UniVap, Avenida Shishima Hifumi, 2911, Urbanova, São José dos Campos, SP 12244-000, Brazil
e-mail: amartin@univap.br

K. J. Jalkanen
Department of Physics, Quantum Protein (QuP) Center, Technical University of Denmark, DTU, 2800 Kgs. Lyngby, Denmark

R. A. Bitar · H. S. Martinho
Centro de Ciências Naturais e Humanas (CCNH), Universidade Federal do ABC, UFABC, Rua Santa Adélia, 166, Bangu, Santo André, SP 09210-170, Brazil

LDA	Linear discriminant analysis
NTT	Normal tissue transcutaneous
PCA	Principal component analysis
THz	Terahertz

1 Introduction

Worldwide, breast cancer is the second leading cause of cancer deaths in women (after lung cancer) and is the most common type of cancers among women [1]. Early detection and effective treatment are crucial to increase the survival rate for breast cancer. Statistical studies indicate that breast cancer is increasing in both developed and developing countries. In Brazil, according to the National Institute for Cancer (INCA), the estimated number of new cases of this kind of cancer expected in 2010 will be 49,240 with an estimated risk of 49 cases per 100 thousand women [2].

The most common technique to detect breast cancer is screening mammography, which is a low-dose X-ray examination. This technique quantitatively probes density changes in breast tissue. However, this technique is dependent only on the morphology and density of the specimen, not on the chemical constituency, leading to no definitive criteria for distinguishing malignant from benignant tissue. This limitation in the lesion discrimination, where only around 30% of the biopsied areas are malignant, leads to the increase in the number of unnecessary biopsy procedures [3, 4]. The risk of repeated exposure to harmful ionizing radiations is also identified as a concern for this method. Due to the failure of the mammographically detected lesions to be definitively determined to be malignant, other diagnosis techniques may be required/necessary, for example, ultrasound and magnetic resonance imaging, further increasing the patient's stress.

In order to alleviate these problems, optical spectroscopic techniques such as fluorescence, diffuse reflectance, infrared, and Raman scattering spectroscopies and imaging are being used and developed for the detection of alterations in both normal and cancerous tissues [5–10]. These techniques can provide information about the composition of tissue at a molecular level, are not destructive, and are less invasive than current diagnostic procedures. Among these techniques, Raman spectroscopy can provide the most detailed information about the molecular composition, molecular structures, conformational and structural changes, aggregation, and inter- and intra-molecular interactions within the tissue under study [11]. Presently, the so-called fingerprint region (400–2,000 cm^{-1}) of the Raman spectrum has been more studied due to the more detailed and very rich information content about the molecules of the tissue in the vibrational modes in this region of the infrared and Raman spectra [10, 12–15]. More recently, the even lower-frequency region of the infrared and Raman spectra, the so-called terahertz region, has been suggested as being rich in information content concerning low-frequency torsional modes that change significantly as a function of secondary, tertiary, and quaternary structure, level of hydration, and the environment in close contact with the biomolecules. Whether the terahertz region [0.1–3.0 THz (3–100 cm^{-1})] will also be useful in medical diagnosis, like the mid-IR/Raman (fingerprint) and high-IR/Raman regions, is yet to be documented.

For in vivo measurements, an optical fiber is needed to deliver the laser light to the tissue and collect the scattered Raman signal. However, the strong Raman signal generated by the Si optical fiber in the fingerprint region has been a problem to date. Here, the Raman signal from the tissue is masked by the strong Raman signal generated by the optical fiber, which is more intense than the tissue Raman signal by at least 1 or 2 orders of magnitude. This complicates the signal analysis of the tissue spectra, requiring complex designs of fiber-optic probes for suppressing the fiber signal [16]. A solution to this is to use the high frequency (HF) Raman region (2,400–3,800 cm^{-1}). In addition to avoiding the inherent fiber Raman signal, another advantage of using the high-energy region is that the Raman scattering in this region due to modes of the biomolecules are generally more intense than those in the fingerprint region. However, the spectral features are strongly overlaping and in many cases anharmonic, which makes the analysis of the modes more complicated.

The use of the HF region in biological tissue investigations is increasing since this region can also provide diagnostic information, that is, be used to correctly identify and distinguish between normal and cancer tissues. Several studies have demonstrated the efficacy of HF optical spectroscopy for diagnosing cancer and other biomedical applications [17–19]. In addition, the use of the HF region for in vivo applications has the advantage of not containing the intrinsic fiber-optic Raman signal.

Here, we report the results of Raman scattering in the HF region for three different types of measurements on mammary rat tissue: in vivo transcutaneous, in vivo skin-removed, and ex vivo biopsy. Breast cancer in the animal model has been shown to be similar to human mammary cancer and therefore can be used [20–22].

The aim of this work was to explore the use of the HF Raman region and multivariate statistical analysis methods, such as principle component analysis (PCA) and linear discriminant analysis (LDA), to distinguish cancer from normal tissue. A comparison between sensitivity and specificity for the three different measurement protocols is discussed.

2 Experiment

This research was in accordance with the policies, rules, and the ethic principles of the Brazilian College of Animal Experimentation (COBEA) that regulate research and experimentation involving animals and was approved by the Ethical Committee of the Universidade do Vale do Paraíba (A022/CEP/2006).

2.1 Sample preparation

A group of twenty 40-day-old virgin Sprague–Dawley female rats with an average weight of 175 ± 10 g was studied. Food and water were provided at libitum.

Mammary gland tumors were induced in 15 rats by a single-dose administration of 50 mg/kg of DMBA (7,12-dimethylbenz(a)anthracene) diluted in 1 mL of soy oil given intragastrically by gavages [20]. The control group of 5 rats was each given, intragastrically by gavages, only soy oil in an amount equal to the solution given to the DMBA group. The mammary glands (6 pairs) of each rat were checked by visual and physical examinations (palpation) three times a week. Within 7 weeks of drug injection, palpable tumors with average diameters between 0.8 and 1.0 cm were detected in at least one of the six breasts of the DMBA group rats, and no tumors were found in the breasts of the control group rats.

Raman spectral measurements were performed in three different ways: (1) Using a Raman fiber-optic probe (RamProbe-Bruker®), spectra were acquired from in vivo normal (NTT-Normal tissue transcutaneous) and cancer (CTT-Cancer tissue transcutaneous) mammary tissues through the shaved skin (in vivo transcutaneous measurement); (2) in the same regions (normal and cancer), skin was locally removed by surgery and spectra were collected using the same Raman probe from normal (IVNT-In vivo normal tissue) and cancer (IVCT-In vivo cancer tissue) tissue (in vivo skin-removed measurement); (3) after killing the rats, the tissue from the measurement regions was surgically removed, labelled and snap-frozen in liquid nitrogen using cryogenic vials (Nalgene®). For subsequent FT-Raman measurements, tissue samples were brought to room temperature and kept moistened in a 0.9 percent physiological solution to preserve their structural characteristics, and three different points/sites of each sample were chosen to be measured. After Raman analysis, the samples were placed in a 10% formaldehyde solution for pathological analysis. The tissue samples were classified histologically as malignant (EVCT-Ex Vivo Cancer Tissue), benign (HM: mammary hyperplasia), or normal (EVNT-Ex Vivo Normal Tissue) tissues. HM was not considered in the statistical analysis due to small number of samples.

2.2 Instrumentation

The Raman scattered light was analyzed with a FT-Raman spectrometer (Bruker RFS 100/S) equipped with a Ge detector and a 1,064 nm Nd/YAG laser as excitation light source. The spectrometer resolution was set to 4 cm^{-1}, and the spectra were recorded with 600 scans for the whole spectral region (900–4,000 cm^{-1}) and only 200 scans for the high-frequency region (2,800–3,600 cm^{-1}). In vivo measurements were taken using a fiber-optic probe (RamProbe, Brucker®), which delivers a power of 120 mW to the sample and collects the scattered light to the spectrometer. For in vivo transcutaneous, the skin thickness of the rat is about 0.8 mm. In the lesion, due to stretching, it is only 0.5 mm. The penetration of the laser is about 1 mm meaning that a small portion of the lesion is probed compared with measurements without skin. An aluminum sample holder was used for ex vivo measurements with the FT-Raman spectrometer. Measurements were taken in the frequency range between 2,800 and 3,600 cm^{-1}. The laser spot size was 200 μm in diameter, and the power was kept below 110 mW at the sample to better preserve the integrity of the samples and prevent photodecomposition caused by the laser beam irradiation.

2.3 Data analysis

In order to remove the background signal, a straight-line fit has been performed by Matlab 6.1 software and subtracted for all Raman spectra [23]. Subsequently, all spectra were normalized (vector normalization: mean subtraction and divided by the standard deviation) and statistically analyzed by using the multivariate statistical tool box of the Minitab 14.20 software. To reduce the dimensionality of the data set, a PCA was used in the Raman spectral range from 2,800 to 3,600 cm^{-1}. The data classification method was based on LDA, which is a prediction method to separate the different groups involved [24].

3 Results and discussions

Figure 1 displays the comparison of average spectra of normal and cancer tissue in the selected HF region for three different measurements: (a) in vivo transcutaneous, (b) in vivo skin-removed, and (c) ex vivo biopsy. In order to compare the transcutaneous measurements, a pure skin spectrum was added to Fig. 1a. Table 1 shows the assignments of tissues Raman spectra for the selected HF interval. Prominent Raman bands at ~2,854 cm^{-1} and 2,895 cm^{-1} (CH_2 stretching of lipids), 2,937 cm^{-1} (CH_3 stretching of proteins), 3,010 cm^{-1} (=CH stretch lipids), and a broad band of water in the region of 3,100–3,550 cm^{-1} are clearly observed in both normal and cancer tissues with a variation

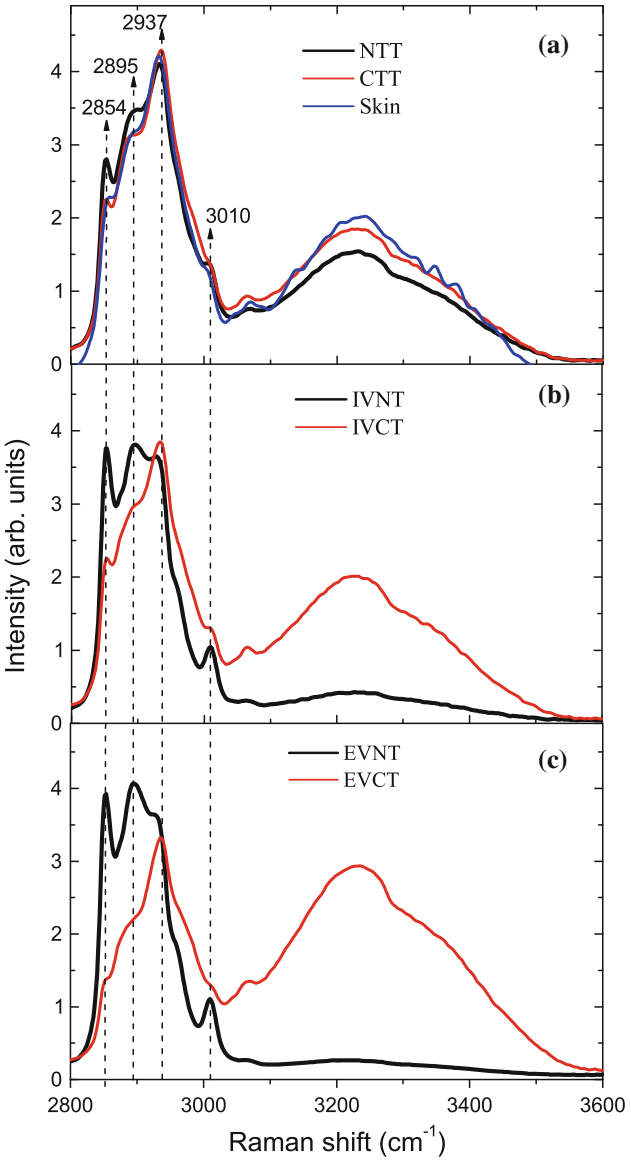

Fig. 1 Comparison of mean spectra of normal and cancer tissue in a selected HF region for the three different ways measured. **a** Normal (NTT) and cancer (CTT) in vivo transcutaneous and pure skin, **b** normal (IVNT) and cancer (IVCT) in vivo skin-removed, and **c** normal (EVNT) and cancer (EVCT) ex vivo biopsy

in intensities [25–27]. This intensity variation can lead to a comparison between normal and cancer tissue spectra based on vibrational spectra of lipids and proteins in the two different tissues.

As shown in Fig. 1, a significant difference is observed between normal and cancer tissues. The intensity of the bands associated with lipid structures (bands around 2,854, 2,895, and 3,010 cm^{-1}) is stronger for normal tissue than that for cancer tissue. On the other hand, the spectra of IVCT and CTT have a larger contribution from the protein band around 2,937 cm^{-1} than the normal tissue, but this is not true for EVCT.

Table 1 Assignments of tissue Raman spectra for a selected HF region [25]

Peak position (cm^{-1})	Major assignment
2,817–2,849	υ_s CH_2 symmetric stretch of lipids
2,840–2,875	υ_s CH_3 symmetric stretch of lipids
2,876–2,919	υ_{as} CH_2 asymmetric stretch of lipids and proteins
2,913–2,938	CH stretch of lipids and proteins
2,928	υ_s CH_3 symmetric stretch due primarily to proteins
2,960	Out-of-plane chain end antisymmetric CH_3 stretch band
2,970	υ_{as} CH_3 asymmetric stretch of lipids, fatty acids
3,008	υ_{as} (=C–H) asymmetric stretch of lipids, fatty acids
3,011	υ (=C–H) stretch of lipids
3,232	O–H and N–H stretching vibrations
3,350–3,550	O–H stretching vibrations

In fact, in contrast to normal cells, cancer cells never stop dividing during their lifetime, which leads to a gradual loss of genetic information. As far as the continuation of reproduction processes is concerned, the malignant cells become more and more primitive and tend to reproduce more quickly and even more haphazardly. During these uncontrolled growth processes, cells synthesize large amounts of proteins, which are essential for the modulation and maintenance of cellular activities. From Fig. 1, one can observe that the water Raman signal in the frequency region from 3,100 to 3,550 cm^{-1} is larger in cancer tissue than in normal and benign tissues. A more significant difference in the water concentration between normal and cancer tissues is observed for in vivo skin-removed, as shown in Fig. 1b, and ex vivo biopsy, as shown in Fig. 1c, measurements, while a smaller difference is observed for in vivo transcutaneous measurements possibly due to the influences of skin, as shown in Fig. 1a. The phenomenon of an increased intensity of the water band in breast cancer tissue that we report can be explained by protein-rich, water-rich cancer cells. One explanation for this result is the presence of an overexpression of the aquaporin1 (AQP1) protein in breast cancer tissue. Aquaporin (AQP) is a water channel protein that facilitates water flux across cell membranes. It is widely expressed in a variety of human malignancies, e.g., tumors of the brain, prostate, lung, ovary, colon, and breast [28]. Because AQPs transport water, most expression studies speculate that AQPs in tumor cells allow water to rapidly penetrate into the growing tumor mass. AQP1 was significantly associated with poor prognosis in breast carcinomas [29]. The

observed increase in water content seen in other types of cancers by optical spectroscopy has been attributed to either the increased concentration of DNA or the hydration of DNA present due to unfolding process during cell divisions [17, 30–32]. Hence, there have been multiple reasons for the noted increase in the water concentration in the high-frequency Raman region of cancer tissue.

Multivariate statistical analysis was implemented for classification between normal and cancer tissues. Here, all spectra were analyzed by PCA and LDA. These statistical methods have been used with success for distinguishing cancerous tissue from normal and benign tissues based on their Raman spectra [17, 18]. In this study, the PCA method was performed in the frequency range of 2,470–3,600 cm^{-1} by a covariance matrix. Figure 2a displays the loading plot (PC1-PC2) for the transcutaneous Raman measurements. PC1 represents 83% (eigenvalue 5.83) of the data variance, and its main contribution comes from the vibration modes at 2,852, 2,895, 3,011, and 3,232 cm^{-1} whose assignments are shown in Table 1. The second PC had 8% (eigenvalue 0.55) of the data variance, and the major difference was related to changes in the vibrational modes at the region of 2,895, 2,946, and 3,232 cm^{-1} corresponding to lipid (υ_s CH_3), protein (υ_s CH_3), and O–H and N–H stretching vibrations, respectively.

The loading plot graphs of PC1 for the in vivo skin-removed, Fig. 2b, and ex vivo Raman measurements, Fig. 2c, resemble very much the PC1 component of Fig. 2a (transcutaneous measurements) although representing now 86% (eigenvalue 8.23) and 98% (eigenvalue 14.38) of the data variance, respectively. In the Fig. 2b, PC2 with 12% (eigenvalue 1.51) of the data variance show the major changes in the protein and lipid regions, respectively. The PC2 in Fig. 2c represents 2% (eigenvalue 0.23) of the data variance.

Figure 3a, b, and c shows the scatter plots of PC1 versus PC2, documenting the differences in the scores for the three types of measurements. Two principal component scores (PC1-PC2), which represent most of the useful

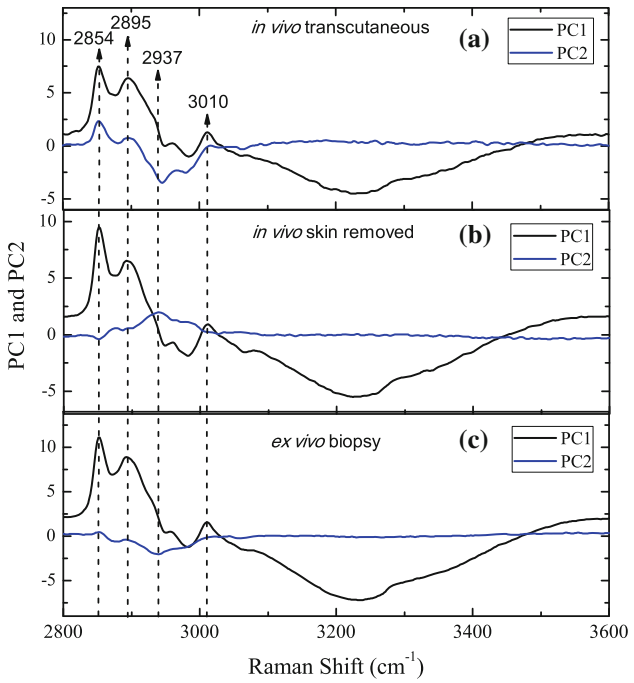

Fig. 2 Loading plot graphs of PC1 to PC2 for: **a** transcutaneous; **b** obtained in vivo skin-removed; and **c** ex vivo Raman measurements applied for classification between normal and cancer mammary tissues

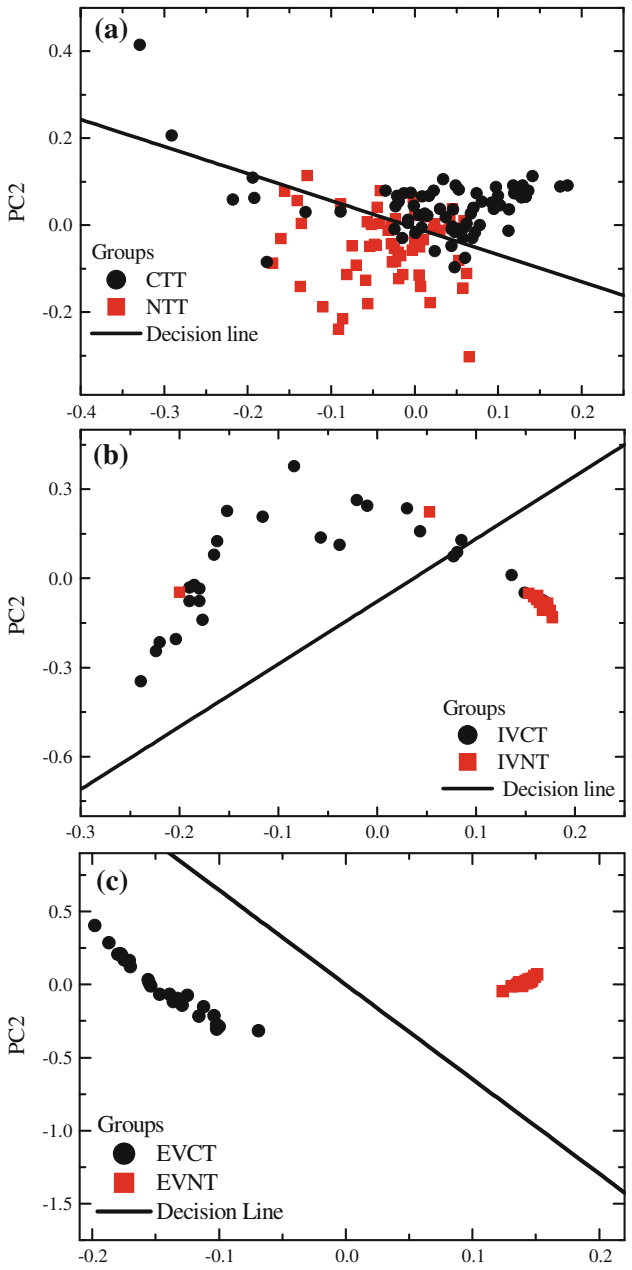

Fig. 3 Scatter plot of PC1 versus PC2 evidencing differences in scores among the three types of measurements, i.e., **a** transcutaneous, **b** in vivo skin-removed and **c** ex vivo biopsy

variance in the data set, were used as input for the LDA. The discriminant analysis was performed by using the cross-validation option. The decision boundary lines between the two classes in Fig. 3 were determined by equating the LDA best-fit functions for each class. Table 2 summarizes the main classifier statistics, that is, shows the results of the discriminant analysis for all Raman spectra (normal and cancer tissue) from the in vivo transcutaneous, in vivo skin-removed, and ex vivo biopsy measurements. From the in vivo transcutaneous statistical analysis with cross-validation, the correct classification for detecting the cancer tissue (sensitivity) is 72.4% and the correct classification for detecting normal tissue (specificity) is 81.2%. These lower values can be explained by the contribution of the skin. LDA analyses with cross-validation for the in vivo skin-removed measurements yielded a diagnostic sensitivity of 81.5% and a specificity of 86.7%. For the ex vivo biopsy, 100% sensitivity and 100% specificity for distinguishing malignant tissue from normal tissues were found. These results can be compared with the values of specificity and sensitivity in the Raman fingerprint region, which were 98 and 99% for ex vivo biopsy [33, 34] and 79 and 85% for in vivo Raman (without skin influence), respectively [35].

The separation between normal and abnormal tissues for measurements without the skin influence is very clear, as shown in Fig. 3b, c, while for transcutaneous measurement is difficult to separate these two types of tissues in the scatter plot as shown Fig. 3a. In Fig. 4, we show the 2-D statistical plots used for testing the PCs of transcutaneous group. Here, the binary logistic regression (BLR) algorithm is used to determine the parameter equation that best differentiated the pathological states using the first 3 PCs. BLR provides a method for modeling a binary response variable, considering values of 0 or 1, and is based on the linear dependence between the logistic function of the probability of response 1 and the diagnosis variable. The BLR model equation is

$$\ln\left(\frac{p}{1-p}\right) = a + \sum_i b_i C_i,$$

where p is the probability of obtaining response 1, a and b_i are the model parameters, and C_i are the diagnosis variables. All these steps were performed using the statistical software Minitab, version 14.20 Minitab Inc®. State College, Pennsylvania, USA. The model's predictive ability was estimated by measuring the association between the response variable and predictive probabilities, the p-values, and the Somer's D parameter. The model was build using a calibration set constituted by half of data. The best model was found to be described by $\ln\left(\frac{p}{1-p}\right) = 1.1 + 18PC1 + 30PC2 + 20PC3$. The goodness of fit tests (Pearson, deviance, and Hosmer–Lemeshow) gave *p*-values between 0.45 and 0.76, which indicated that there was insufficient evidence to claim that the model does not fit the data adequately. Once applied to the testing spectral set, it was found 91,0 pairs concordant to the model. The discordant and ties were 8.8 and 0.2, respectively. The Somer's D parameter was found to be 0.82, which indicates a good level of accordance.

The straight line represents the completely random $p = 0.50$ case, which separates the cancer and normal tissues regions. From the visual inspection is clear the goodness of the fitted model.

In addition to demonstrating the possibility for distinguishing cancer from normal tissue based on Raman spectra, our results show the efficacy of studying the HF region of biological tissues. One advantage is that tissue Raman spectra do not have contributions from optical fiber signals, favoring the use of basic designs of fiber-optic probes. The more intense tissue Raman signals compared with the fingerprint region (400–2,000 cm^{-1}) provide another advantage for studying the HF region of tissue Raman spectra, leading to a threefold reduction in the acquisition time, which is critical for medical applications. This suggests and documents the feasibility of possibly using fiber-optic coupled FT-Raman spectroscopy in the HF Raman spectra region for in vivo and ex vivo tissue diagnosis purposes, including but not limited to the applications investigated in this work.

Table 2 Sensitivity and Specificity calculated using LDA results

Experimental measurement	Sensitivity (%)	Specificity (%)
In vivo transcutaneous	72.4	81.2
In vivo skin-removed	81.5	86.7
Ex vivo biopsy	100	100

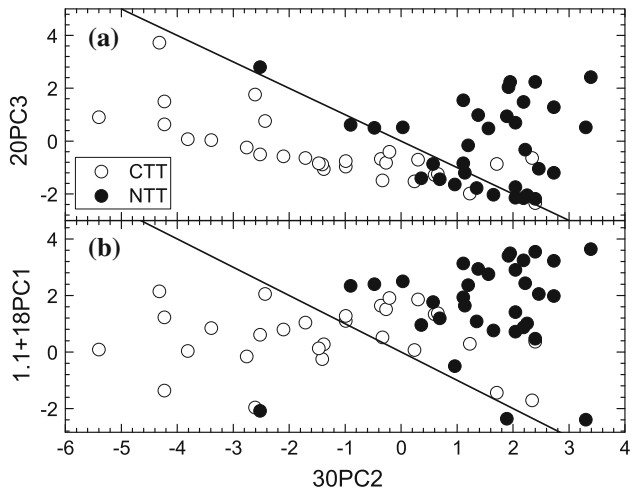

Fig. 4 2-D statistical plots used for testing the PCs for use in breast cancer diagnostics

4 Conclusions

In summary, a HF Raman spectroscopy study for in vivo and ex vivo measurements of normal and cancer breast tissue, associated with the multivariate statistical analysis method, has been reported in this work. Mean Raman spectra of normal and cancer breast tissue showed significant differences in bands characteristic of lipid and protein structures as well as in the broad bands due to water. By using Raman measurements and the PCA and LDA methods on all HF Raman spectra, a good discrimination between cancer and normal breast tissue was obtained. Tissue Raman signals more intense and free of optical fiber signals, compared with the fingerprint region, make of Raman spectroscopy in the HF region a nondestructive and noninvasive potential tool for in vivo and ex vivo measurements of cancer tissue. It is highly likely that measurements on other altered states of biological tissues will also show that the HF Raman region can be used as a diagnostic tool. HF region will provide molecular-level information on not only concentration of the biomolecules but also the secondary and tertiary structures and level of hydration.

Acknowledgments Authors thank L.N.Z. Ramalho and F.S. Ramalho for inducing cancer in the rats that were used in this study. Thanks go to FAPESP and CNPq for financial support for projects 01/14384-8, 301362/2006-8, and 302761/2009-8, and to FAPESP for project 16782-2/2009, which allowed Prof. Jalkanen to visit LEVB at UniVaP for the period from June 2010 to May 2011 from the Quantum Protein (QuP) Center at the Technical University in Denmark. Finally, we thank the reviewers of our work for their comments, recommendations, and suggestions.

References

1. Global cancer facts and figures (2007) American Cancer Society, 2007
2. INCA (2009) Instituto Nacional do Câncer. Incidência de câncer no Brasil. Avaiable at http://www.inca.org.br
3. Johnson JM, Dalton RR, Wester SM, Landercasper J, Lambert PJ (1999) Histological correlation of microcalcifications in breast biopsy specimens. Arch Surg 134:712–716
4. Evans AJ, Wilson ARM, Burrell HC, Ellis IO, Pinder SE (1999) Mammographic features of ductal carcinoma in situ (DCIS) present on previous mammography. Clin Radiol 54:644–646
5. Zhu CF, Burnside ES, Sisney GA, Salkowski LR, Harter JM, Yu B, Ramanujam N (2009) Fluorescence spectroscopy: an adjunct diagnostic tool to image-guided core needle biopsy of the breast. IEEE Trans Biomed Eng 56:2518–2528
6. Volynskaya Z, Haka AS, Bechtel KL, Fitzmaurice M, Shenk R, Wang N, Nazemi J, Dasari RR, Feld MS (2008) Diagnosing breast cancer using diffuse reflectance spectroscopy and intrinsic fluorescence spectroscopy. J Biomed Opt 13:024012
7. Movasaghi Z, Rehman S, Rehman IU (2008) Fourier transform infrared FTIR spectroscopy of biological tissues. Appl Spectrosc Rev 43:134–179
8. Bitar RA, Martinho HS, Tierra-Criollo CJ, Ramalho LNZ, Netto MM, Martin AA (2006) Biochemical analysis of human breast tissues using Fourier-transform Raman spectroscopy. J Biomed Opt 11:054001
9. Hanlon EB, Manoharan R, Koo T-W, Shafer KE, Motz JT, Fitzmaurice M, Kramer JR, Itzkan I, Dasari RR, Feld MS (2000) Prospects for in vivo Raman spectroscopy. Phys Med Biol 45:R1–R59
10. Wills H, Kast R, Stewart C, Sullivan B, Rabah R, Poulik J, Pandya A, Auner G, Klein MD (2009) Diagnosis of Wilms' tumor using near-infrared Raman spectroscopy. J Pediatric Surg 44:1152–1158
11. Tu AT (1982) Raman spectroscopy in biology. John Wiley & Sons, New York
12. Chowdary MVP, Kumar KK, Mathew S, Rao L, Krishna CM, Kurien J (2009) Biochemical correlation of Raman spectra of normal, benign and malignant breast tissues: a spectral deconvolution study. Biopolymers 91:539–546
13. Haka AS, Shafer-Peltier KE, Fitzmaurice M, Crowe J, Dasari RR, Feld MS (2005) Diagnosing breast cancer by using Raman spectroscopy. PNAS 102:12371–12376
14. Marzullo ACM, Neto OP, Bitar RA, Martinho HS, Martin AA (2007) FT-Raman spectra of the border of infiltrating ductal carcinoma lesions. Photomed Laser Surg 25:455–460
15. Shim MG, Song L-MWK, Marcon NE, Wilson BC (2000) In vivo near-infrared Raman spectroscopy: demonstration of feasibility during clinical gastrointestinal endoscopy. Photochem Photobiol 72:146–150
16. Santos LF, Wolthuis R, Koljenovic S, Almeida RM, Puppels GJ (2005) Fiber-optic probes for in vivo Raman spectroscopy in the high-wavenumber region. Anal Chem 77:6747–6752
17. Mo J, Zheng W, Low JJH, Ng J, Ilancheran A, Huang Z (2009) High wavenumber Raman spectroscopy for in vivo detection of cervical dysplasia. Anal Chem 81:8908–8915
18. Nijssen A, Maquelin K, Santos LF, Casper PJ, Schut TCB, den Hollander JC, Neumann MHA, Puppels GJ (2007) Discriminating basal cell carcinoma from perilesional skin using high wavenumber Raman spectroscopy. J Biomed Opt 12:034004
19. Koljenovic S, Schut TCB, Wolthuis R, de Jong B, Santos L, Casper PJ, Kros JM, Puppels GJ (2005) Tissue characterization using high wave number Raman spectroscopy. J Biomed Opt 10:031116
20. Barros C, Muranaka EN, Mori LJ, Pelizon CH, Iriya K, Giocondo G, Pinotti JA (2004) Induction of experimental mammary carcinogenesis in rats with 7, 12-dimethylbenz(a)anthracene. Revista do Hospital das Clínicas 59:257–261
21. Russo J, Russo IH (2006) The role of estrogen in the initiation of breast cancer. J Steroid Biochem Mol Biol 102:89–96
22. Costa I, Solanas M, Escrich (2002) Histopathologic characterization of mammary neoplastic lesions induced with 7, 12 dimethylbenz(alpha) anthracene in the rat—A comparative analysis with human breast tumors. Arch Pathol Lab Med 126:915–927
23. Lieber CA, Mahadevan-Jansen A (2003) Automated method for subtraction of fluorescence from biological Raman spectra. Appl Spectrosc 57:1363–1367
24. Oliveira AP, Bitar RA, Silveira LJ, Zangaro RA, Martin AA (2006) Near-infrared Raman spectroscopy for oral carcinoma diagnosis. Photomed Laser Surg 24:348–353
25. Movasaghi Z, Rehman S, Rehman IU (2007) Raman spectroscopy of biological tissues. Appl Spectrosc Rev 42:493–541
26. Bitar RA, Martinho HS, Tierra-Criollo CJ, Ramalho LNZ, Netto MM, Martin AA (2006) Biochemical analysis of human breast tissues using Fourier-transform Raman spectroscopy. J Biomed Opt 11:054001
27. Krishna CM, Kurien J, Mathew S, Rao L, Maheedhar K, Kumar KK, Chowdary MVP (2008) Raman spectroscopy of breast tissues. Expert Rev Mol Diagn 8:149–166

28. Hu J, Verkman AS (2006) Increased migration and metastatic potential of tumor cells expressing aquaporin water channels. FASEB J 20:1892–1894
29. Otterbach F, Callies R, Adamzik M, Kimmig R, Siffert W, Schmid KW, Bankfalvi A (2010) Aquaporin 1 (AQP1) expression is a novel characteristic feature of particularly aggressive subgroup of basal-like breast carcinomas. Breast Cancer Res Treat 120:67–76
30. Hornung R, Pham TH, Keefe KA, Berns MW, Tadir Y, Tromberg BJ (1999) Quantitative near-infrared spectroscopy of cervical dysplasia in vivo. Human Reprod 14:2908–2916
31. Kondepati V, Heise H, Backhaus JJ (2008) Recent applications of near-infrared spectroscopy in cancer diagnosis and therapy. Anal Bioanal Chem 390:125–139
32. Wood BR, Chiriboga L, Yee H, Quinn MA, McNaughton D, Diem M (2004) FTIR mapping of the cervical transformation zone, squamous and glandular epithelium: search for the elusive infrared cancer markers. Gynecol Oncol 93:59–68
33. Moreno M, Raniero L, Arisawa EAL, Santo AME, Santos EAP, Bitar RA, Martin AA (2010) Raman spectroscopy study of breast disease. Theor Chem Acc 125:329–334
34. Haka AS, Volynskaya Z, Gardecki JA, Nazemi J, Lyons J, Hicks D, Fitzmaurice M, Dasari RR, Crowe JP, Feld MS (2006) In vivo margin assessment during partial mastectomy breast surgery using Raman spectroscopy. Cancer Res 66:3317–3322
35. Draga ROP, Grimbergen MCM, Vijverberg PLM, van Swol CFP, Jonges TGN, Kummer JA, Bosch JHR (2010) In vivo bladder cancer diagnosis by high-volume Raman spectroscopy. Anal Chem 82:5993–5999